Physical characterization of hafnium aluminates dielectrics deposited by atomic layer deposition

Danilo R. Huanca[1], V. Christiano[1], C. Adelmann[2], Patrick C. Verdonck[2] and Sebastião G. dos Santos Filho[1]

[1]LSI/PSI/EPUSP, Av. Prof. Luciano Gualberto,158, 05508-900 São Paulo, SP, Brasil
[2]IMEC, Kapeldreef 75, B-3001 Leuven, Belgium
e-mail: droqueh@usp.br

ABSTRACT

Hafnium aluminates films with 50 mol% of Hf were deposited onto Si(100) using atomic layer deposition. The films were annealed by RTP at 1000 °C for 60 s in pure N_2 or N_2+5%O_2 and by LASER at 1200°C for 1ms in pure N_2. Then, they were characterized by X-ray spectroscopies, ellipsometry, Rutherford backscattering and scanning electron microscopy. For thin films annealed by RTP in N_2, phase separation takes place, promoting the formation of HfO_2 and $Al_{2.4}$ $O_{3.6}$ crystalline phases. In contrast, the films annealed by LASER remain predominantly amorphous with crystalline facets of $Al_{2.4}O_{3.6}$. Also, non-homogeneous distribution of the chemical elements within the dielectrics gave rise to the formation of several regions which can be viewed as sub-layers, each of them with arbitrary electron density and thickness. As a result, Kratky curves pointed out to the coexistence of different features described by different gyration radius yielding GISAXS scattering profiles with polydispersive characteristics. Finally, the samples annealed by RTP were interpreted as agglomerates of spheroids with different sizes (1.1-2.2 nm) and with different crystalline phases whereas the samples annealed by LASER were interpreted as larger spheroids of crystalline $Al_{2.4}O_{3.6}$ (1.7-2.7nm) embedded in a matrix predominantly amorphous.

Index Terms: Thin dielectric films, Physical characterization, X-ray spectroscopy.

I. INTRODUCTION

In the last years, the main material used as gate dielectric for field effect transistors (FET) has been the silicon oxynitrides [1,2]. Due to the continuous scaling down of the CMOS devices, the substitution of the silicon oxynitride as gate material became mandatory because thinner films of silicon oxynitride lose their dielectric properties when the thickness achieves dimensions less than 1nm and present increase of the leakage current due to direct tunneling [1-4]. In order to overcome this difficulty, different high-*k* dielectric composed by binary and ternary compounds were proposed to substitute it [1-4]. One dielectric which belongs to this set of high-k dielectric is the hafnium oxide (HfO_2). It is usually deposited on silicon substrate using different methods such as sputtering, atomic layer deposition (ALD), metalorganic chemical vapor deposition, pulsed laser and so on [1,3-6]. Although the dielectric constant of HfO_2 is larger ($k \approx 20$), the main drawback of this material is its relatively low crystallization temperature (≈ 500 °C) [1,2,7,8]. Crystalline phases of HfO_2 are undesirable because promotes an unstable silicon/metal oxide interface due to the electric and mass transfer [9] as well as the coexistence of different crystalline phases in the bulk of the film give rise to an anisotropy of the dielectric constant [10,11]. In order to maintain the HfO_2 in its amorphous phase even during thermal treatments in conventional CMOS processing, hafnium silicates (1,12) or hafnium aluminates [1,9,13-15] has been used for increasing the crystallization temperature. Also, this procedure may give rise to the phase separation within the dielectric matrix at higher temperatures (> 1000 °C) by forming centers of scattering like agglomerates and crystallites for concentration of aluminate higher than 30 mol% [12-15].

In addition, rapid thermal annealing has been employed in order to control the thermal budget the samples are submitted to. Hafnium aluminates with different molar concentrations of aluminum were submitted to RTP at higher temperature (> 1000 °C) and different molar concentrations of aluminum (0 – 70 mol%) [12]. On the other hand, flash laser annealing allows one to substantially diminish the thermal budget and, as a consequence, diffusion of species although the full wafer depth and surface are achieved. This technique will be used at the first time in this work in order to analyze its influence on the phase separation [16].

The characterization of thin films requires advanced techniques such as scanning electron microscopy (SEM), transmission electron microscopy (TEM) [9,12-15,17], Rutherford backscattering spectroscopy (RBS) [16] and those based in X-ray spectroscopy [17-20] as well as other complementary techniques [21]. However, this task may not be easy because the equipments used for the physical characterization must be adjusted for thin films [17-21]. For instance, the beam for X-ray diffraction should be irradiated almost parallel to the film surface and is known as Grazing incidence X-ray diffraction (GIXRD). On the other hand, grazing incidence scattering X-ray spectroscopy (GISAXS) is a powerful technique to investigate phase separation by obtaining the characteristic wavelength in the plane of the films and the characteristic sizes in the film morphology represented by gyration radius [19,20]. In this paper we report the physical characterization of hafnium aluminate thin films deposited by ALD technique and annealed at different conditions in order to analyze the undesired crystallization and phase separation.

II. EXPERIMENTAL PROCEDURE

Hafnium aluminates films were deposited on silicon substrate by ALD technique with 50 mol% of Hf ($Hf_xAl_{1-x}O_y$, x=0.5). Layers were deposited in an ASM Pulsar 3000 connected to a Polygon 8300 Platform on Si (100) wafers, on which a 1 nm thick chemical oxide has been grown (IMEC clean) [22]. The precursors were $HfCl_4$ and $Al(CH_3)_3$, in combination with H_2O as oxidants. The deposition conditions were adjusted to achieve thin homogeneous films 15 nm thick. Following, the layers were annealed on full wafers at IMEC using an ASM Levitor 4300 for spike annealing at 1000 °C during 60 s in ultrapure N_2 (sample G1) and N_2+5% O_2 (sample G2)and an AMAT laser annealing chamber for laser annealing at 1200 °C during 1 ms (sample G3). Annealing temperature above 1000 °C was chosen because the conventional CMOS processes are usually made at this temperature, so the amorphous dielectric used as gate must have thermal stability and sharp interface [1,2,8].

Grazing Incidence Small Angle X-ray Spectroscopy (GISAXS) experiments were performed at the XRD2 X-ray beam line of the Brazilian Synchrotron Light Laboratory (LNLS) using a 0.1749 nm wavelength beam. The two-dimensional patterns of the GISAXS intensity were recorded following the procedure proposed by Salditt et al. [23], in which the incidence angle of the X-ray beam on the multilayer external surface is kept constant and the two-dimensional scattering intensity is measured using a (10 x 10) cm^2 imaging plate with a 10^6 dynamical range and a (0.2 x 0.2) mm^2 pixel size.

The morphological features of the films were investigated by XRR, SEM, RBS and ellipsometry, whereas the phase separation was analyzed by GIXRD and GISAXS techniques. GIXRD employed an X-ray beam with λ= 0.1542 nm at an incidence angle of 0.7° to obtain the formed crystalline phases. On the other hand, GISAXS permitted to obtain scattering contributions with in-plane information at the horizontal and vertical directions, q_y and q_z, respectively, which are given by [19,20]:

$$q_y = \frac{2\pi}{\lambda}\sin\beta\cos\alpha_f \tag{1}$$

and,

$$q_z = \frac{2\pi}{\lambda}\left(\sin\alpha_i + \sin\alpha_f\right) \tag{2}$$

where β is the horizontal scattering angle and α_f is the vertical scattering angle and α_i is the incident grazing angle.

The two-dimensional GISAXS pattern (2D-GISAXS) was transformed to one-dimensional ones (1D-GISAXS). The 1D-GISAXS profiles were extracted along the q_y direction for different q_z points, then they were converted to the Kratky curves (Iq_y^2 x q_y) [24-26] to obtain the morphological features after phase separation by modeling the shapes of agglomerates or crystallites as spheroids with different dimensions.

RBS spectra were taken at 2.2 MeV under normal incidence of a $^4He^+$ beam and with a scattering angle of 170° using an accelerator Pelletron - Tanden, model 55 DH/NEC and the spectra were fitted with the aid of the SIMNRA 6.0 code[27] using a multilayer approach.

Table I summarizes the annealing and the results of thickness obtained from ellipsometry, XRR and SEM.

Ellipsometry with λ= 628.3 nm was used to measure the thickness and refractive index at ten different points on the film surface and the average value of them is shown as T_{El} in Table I. Cross-section images of the films were obtained using the secondary electron method in ultrahigh resolution mode of the NANOSEM electron microcopy (UHRSEM). The standard deviation of ellipsometric measurement was less than 0.62 nm, while in the case of the SEM measurement was about 0.8 nm.

Table I. Annealing procedure, critical angle and thickness of the hafnium aluminates obtained from XRR, ellipsometry and SEM.

Film	Annealing procedure	q_c (°)	T_{XRR} (nm)	T_{El} (nm)	T_{SEM} (nm)
G1	1000ºC, 60s, N_2 (RTP)	0.414	15.22	17.2	16.5
G2	1000ºC, 60s, N_2 + 5% O_2 (RTP)	0.400	15.24	16.0	16.7
G3	1200ºC, 1ms, N_2 (LASER)	0.409	14.81	17.3	16.3

III. RESULTS AND DISCUSSIONS

A. Morphological analysis by X-ray reflectometry (XRR)

Fig 1 shows the XRR curves in the reciprocal space with a typical wavy appearance known as Kiessig fringes [17,18,28,29]. These fringes appear due to the interference effect of the beams reflected at the air/dielectric and dielectric/silicon interfaces [28,29]. The periodicity of these ondulations is related to the dielectric thickness, while the fall rate is influenced by the roughness of both interfaces [17-19,21].

An estimation of the thickness, valid for homogeneous films, were made using the relation $T_{XRR}=2\pi/\Delta q_z$ [23], while their critical angle (θ_c) were obtained from the XRR spectra using the criteria of the 50% of the first decay [28]. Table I shows T_{XRR} varying from 14.82 to 15.24 and, is of the same order of the expected value for ALD deposition conditions. θ_c was about 0.40° and the lowest value was obtained for films annealed by LASER. It is important to point out that ellipsometry leads to thickness slightly higher compared to XRR possibly because it can not take into account the interface roughness or electron density variation along the film.

In addition, the XRR curves were fitted using the PARRAT32 code [30]. This computational program uses Parrat formalism [31] along with the Névot-Croce factor which take in count the surface roughness effect upon the reflectivity [32]. Mathematically they are expressed as

$$R_j = \frac{r_{j,j+1} + R_{j+1}\exp(it_{j+1}k_{z,j+1})}{1 + r_{j,j+1}R_{j+1}\exp(it_{j+1}k_{z,j+1})} \tag{3}$$

$$r_{j,j+1} = \frac{k_{z,j} - k_{z,j+1}}{k_{z,j} + k_{z,j+1}}\exp(-2\sigma_{j+1}^2 k_{z,j}k_{z,j+1}) \tag{4}$$

$$k_{z,j} = \sqrt{k_{z,0}^2 - 4\pi\rho_j} \tag{5}$$

The reflectivity of the system is given by $R=|R_0|^2$; $R_{N+1}=0$; $R_N=r_{N,N+1}$. In equation (3), t_j and k_j are the thickness and wave number of the j-th layer, respectively, while ρ_j is the complex value of the electron density and σ_j is the roughness of the j-th layer.

Although the films were supposed to be single layer, they could not be fitted using the single layer model, being necessary a four-layer model. The results about the physical thickness and surface roughness are summarized in Table II. In the last row of this Table are summarized the total physical thickness of the films by summing the thicknesses of the four layers employed for fitting. It varies between 14.96 nm and 15.52 nm and they are slightly different of those computed using the relation $T_{XRR}=2\pi/\Delta q_z$ (compare Table I with Table II). The surface roughness of these films was lower than 0.6 nm. Low surface roughness is characteristic of the films deposited by ALD technique as reported in literature [5,6-9,32]. The profile of the electron density of the films (Fig. 2) shows that it is lower for the film annealed by LASER (G3) and varies in depth for all the films, being higher at the surface of all the films. According to these results, during the thermal treatment of the films, at least four layers arise due to the interdiffusion of the different chemical elements from the dielectric layer toward the substrate and vice-versa [1,33]. In this sense, Dai et al [34], report that, in $Hf_xAl_{1-x}O_y$ deposited on Si substrate, interlayer between

Table II. Thickness and Roughness of the thin layers extracted using the four-layer model and the PARRAT32 code.

	G1		G2		G3	
layer	T_j (nm)	σ_j(nm)	T_j (nm)	σ_j(nm)	T_j (nm)	σ_j(nm)
1	1.28	0.57	1.36	0.23	1.52	0.14
2	4.19	0.62	3.86	0.68	4.64	0.51
3	8.78	1.94	9.83	1.51	7.06	1.98
4	1.25	0.84	0.48	0.25	1.74	1.02
total	15.50	-	15.52	-	14.96	-

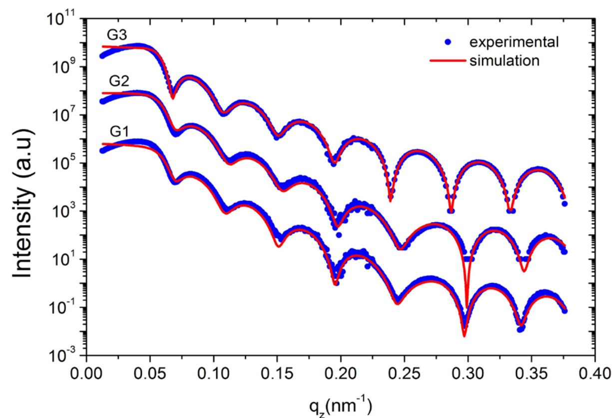

Figure 1. XRR curves for the hafnium aluminate dielectrics annealed by RTP in N_2 (G1) and N_2+5%O_2 (G2) and annealed by laser in N_2 (G3)

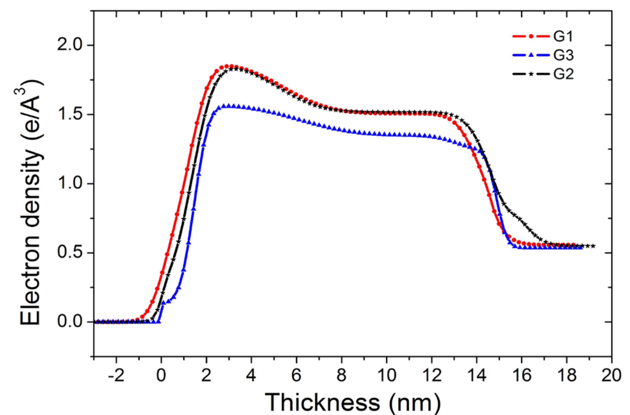

Figure 2. Electron density profile extracted by fitting the XRR curves of dielectrics annealed by RTP in N_2 (G1) and N_2+5%O_2 (G2) and annealed by laser in N_2 (G3)

film and silicon is formed by hafnium silicide compound, which is linked to the larger diffusion of Hf toward the substrate. The formation of this interlayer would be accompanied by the formation of a rougher interface [34]. The results about the thickness layer and roughness of these films (TABLE II) suggest no hafnium silicide formation. The thickness of the films are about 15 nm as projected and have sharp interfaces with lower roughnesses.

Nishimura et al. [9] had been reported that the roughness variation is related to the decomposition of the hafnium aluminate in HfO_2 and Al_2O_3 in which Al_2O_3 remains next to the film surface. For this reason, in films with rougher surface, the concentration of Al_2O_3 may be larger, which supports the higher surface roughness for RTP treated samples (see layer I in Table II).

B. Analysis by Rutherford Backscattering

The typical RBS spectra of the three dielectrics are depicted in Fig. 3 and show that the aluminum signal over the silicon one is clearly evident in the spectrum of the dielectric annealed by LASER. This evidence indicates a larger amount of aluminum next to the film surface, while, for dielectrics annealed by RTP, the aluminum signal became scattered over the silicon signal and reveals that aluminum is distributed along the film and diffused a bit in the Si substrate. The spectra in Fig. 3 were fitted by the SIMNRA 6.0 code [27] using a seven-layer model for the dielectric region – an analogous approach as in the case of the Parrat fitting for XRR curves. The results obtained for the thickness of the dielectrics (T_{RBS}) are summarized in Table III, and the distribution profile of O, Al and Hf as function of the dielectric thickness is depicted in Fig. 4.

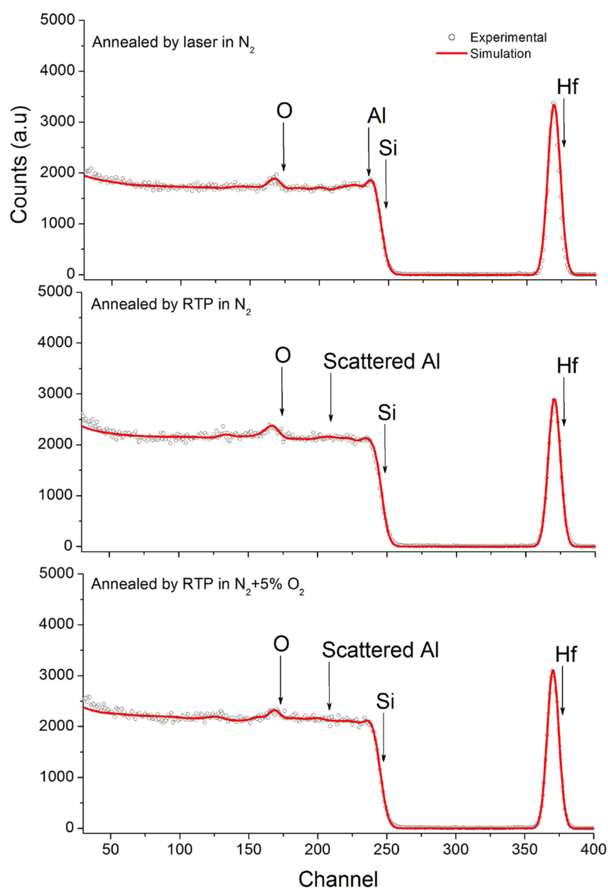

Figure 3. RBS spectra from Hf-based dielectrics annealed by RTP in N_2 (G1) and N_2+5%O_2 (G3) and annealed by LASER in N_2 (G2)

The RBS thickness was computed using an extended version of the relation (equation 6) proposed by Schmid et al. [35] by supposing that the chemical elements which compose the films are distributed homogeneously in each of the seven layers in Table III.

Table III. Physical thickness obtained from RBS spectra of dielectrics using a seven-layer model in the SIMNRA code. The values are in nanometers.

layer	G1	G2	G3
1	1.37	1.77	1.91
2	3.90	3.59	1.72
3	2.66	3.32	2.72
4	2.10	2.65	1.92
5	2.75	2.13	2.11
6	1.35	1.14	2.29
7	1.42	1.16	2.47
total	15.55	15.77	15.14

$$T_{RBS} = \sum_{k}^{7}\sum_{j}^{3} \frac{M_{j,k} n_{j,k,area}}{N_A \rho_{j,k}} f_{j,k} \qquad (6)$$

In equation 6, $M_{j,k}$, $\rho_{j,k}$, $n_{j,k,area}$ and $f_{j,k}$ are the molecular weight, the mass density, the areal density of atoms and the fraction of the j-th element placed within the k-th layer, respectively. N_A is the Avogadro´s number. Both $M_{j,k}$ and $\rho_{j,k}$ were taken from the literature [36], while the $n_{j,k,area}$ and $f_{j,k}$ were furnished by the SIMNRA. The results show that the physical thicknesses of the films T_{RBS} are similar to the T_{XRR} values (Table II) and varies from 15.14 to 15.77 nm (Table III).

The profile of the elements (Fig. 4) reveals that the concentration of aluminum inside the dielectric annealed by RTP (G1) decreases slowly from the surface to the film/silicon interface while for the dielectric annealed by LASER (G3), an abrupt variation is observed next to the surface followed by a slight increase along the bulk. On the other hand, also for the dielectric annealed by RTP, the decrease of the aluminum is accompanied by a concomitant

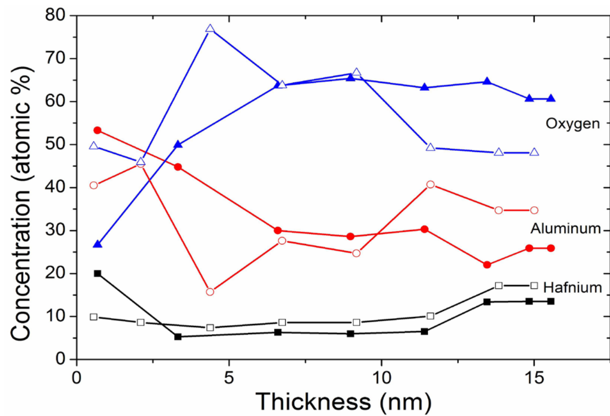

Figure 4. Atomic concentration profiles of the chemical elements distribution as function of the film thickness for the films annealed in N_2 by RTP (full symbols) and LASER (unfilled symbols). Not show for the films annealed in N_2 + 5% O_2 by RTP

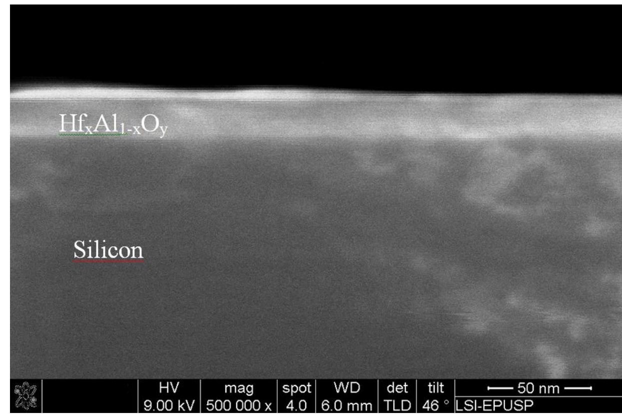

Figure 5. Typical cross-section SEM image of the dielectric annealed in N_2 by RTP.

decrease of hafnium and an increase of oxygen, starting from the surface. This is consistent with gradual phase changing that means a non-homogeneous film in depth. This non-homogeneous distribution of the chemical elements within the dielectric gives rise to the formation of several regions which can be viewed as sub-layers into the dielectric, each of them with arbitrary electron density and thickness. For this reason, their XRR curves can not be fitted by one single model and was necessary a four-layer model, and in the case of the RBS spectra, seven-layer model.

On the other hand, it is noteworthy for the LASER annealed films that the larger amount of aluminum next to the surface run in the lower concentration of oxygen, which is consistent with aluminum-rich phase at the surface. After the abrupt variation of the aluminum, the increase of the aluminum is accompanied by a concomitant decrease of oxygen and hafnium remains almost constant. These observed inhomogeineities along the depth is correlated with the GIXRD spectra in the following.

C. Physical thickness measurement by UHRSEM

As already mentioned, cross-section SEM images of the thin dielectrics were recorded using the secondary electrons method in the high resolution mode. Fig. 5 shows a typical UHRSEM for a dielectric annealed by RTP in N_2 (G1). The physical thicknesses of these films as well as their standard deviation were obtained for each thermal processing (Table I). As a result, the physical thickness was around of 16.5 nm. This result is very close to that obtained by XRR and RBS (The UHRSEM are not shown for G2 and G3 samples).

D. Phase separation analysis by GIXRD

The characterization by GIXRD (Fig. 6) discloses that, after LASER annealing, the film remains almost entirely amorphous with small content of crystalline $Al_{2.4}O_{3.6}$ while, after annealing in N_2 by RTP, the matrix film passes to contain both crystalline $Al_{2.4}O_{3.6}$ and HfO_2. Therefore, phase separation was observed to occur in this last case, which agrees with the profiles of Al, Hf and O presented in Fig. 4. For the RTP annealing, $Al_{2.4}O_{3.6}$ and HfO_2, crystalline facets are supposed to be formed in the region where Al and Hf are decreasing and O is increasing, starting from the film surface. This is inferred by finding the film bulk with roughly 50 mol% (atomic percent) of Hf yet, this is to say, possibly without any significant crystallization. On the other hand, after LASER annealing, the Hf profile remains almost constant at the surface and inside de bulk indicating absence of crystallization to

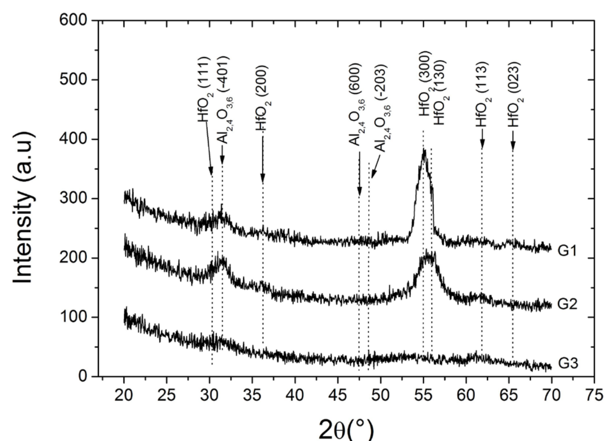

Figure 6. GIXRD spectra of the films annealed by RTP in N_2 (G1) and N_2+5%O_2 (G2), and annealed by LASER in N_2 (G3)

form HfO_2. Also, the Al and O profiles changed in the regions close to the interfaces and may withstand the appearance of $Al_{2.4}O_{3.6}$ crystalline facets. Moreover, the larger peak at 2θ ≈ 31.5° shows that the addition of 5%O_2 in the media increases the formation of crystalline phase of $Al_{2.4}O_{3.6}$, similar to that observed in hafnium aluminates and hafnium silicates [12,13].

In microelectronics applications, high-k dielectric films with amorphous phase is desirable is order to obtain stable silicon/metal oxide interfaces, as well as avoid the anisotropic dielectric constant that can enhance the leakage current [1,10,11]. In this sense, thermal treatment by LASER seems to be better for this task than RTP. In addition, the RBS analysis (Fig. 3) suggests that the phase separation in the film annealed by RTP seems to be linked to the aluminum migration from the dielectric toward the substrate, since, in the case of the LASER annealed film, Al remains almost constant within the film (Fig. 4). In the case of the films annealed by RTP, although Dai et al [34] reports similar results for Al diffusion, the roughness of the film/substrate interface of the films here studied are lower, i.e, the interface was sharp. This difference could be attributed to the deposition method because in [34] the authors use the pulsed-laser deposition method. Although Hf is inward the silicon at some degree (see Fig. 4 for RTP), no peaks of hafnium silicide are observed in GIXRD spectra (Fig. 6). No formation of this compound could explain the sharpness of the film/silicon interface of these films.

E. Phase separation analysis by GISAXS

GISAXS is another technique useful for analyzing phase separation within thin films [19]. Fig. 7 shows GISAXS spectra of the same Hf-based dielectrics depicted in figures 4 and 6. Although similar parameters were used to deposit the films, the shape of these GISAXS spectra were different. In fact, the GISAXS pattern of dielectrics annealed at 1000°C for 60s (G1) and at 1200°C for 1ms (G3) are different among them, showing thus the effect of the thermal annealing upon the final morphology. No significant differences were observed in GISAXS patterns of both films annealed by RTP (Fig. 7a and 7c). Other common feature of these spectra is related to its anisotropy since they are larger in q_y-direction and short in q_z-direction. This anisotropy can be associated to phase separation with a particular distribution of sizes in the film morphology, which can be described by different gyration radius [19,20,37]. In spite of the thermal treatment method, these GISAXS spectra show clearly the Yoneda´s peak placed in $q_z \approx 0.71$ nm^{-1}, labeled by "Y" in Fig. 7. Yoneda´s peak arises when the incident angle of the beam is equal to the critical angle [37,38]. The sharpness of this peak

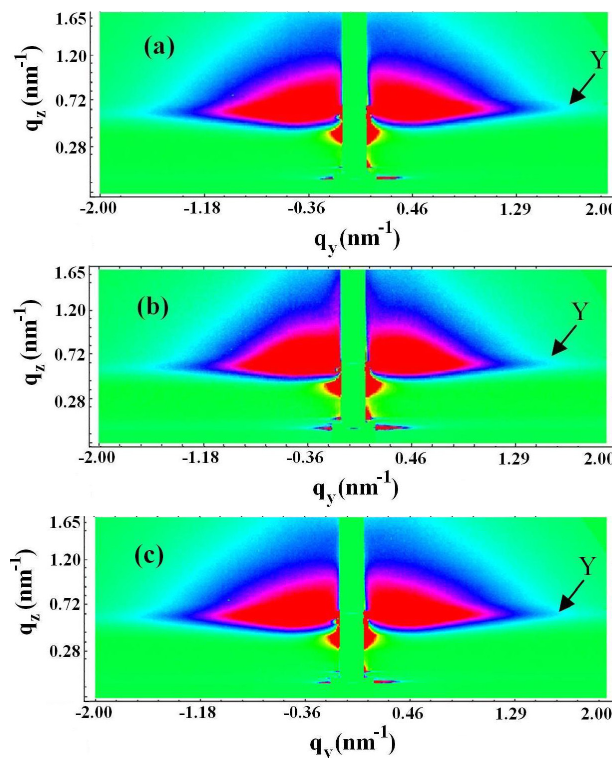

Figure 7. GISAXS pattern of Hf-based dielectrics annealed by RTP at 1000°C for 60s in N_2 (a) at 1000°C for 60s in N_2+5% O_2 (c) and annealed by LASER at 1200 °C for 60s in N_2 (b).

is well correlated to the lowest surface roughness of these films (See Table II). In order to quantify the main features of the morphology, firstly, the two-dimensional GISAXS pattern (2D-GISAXS) was transformed to one-dimensional ones (1D-GISAXS). The 1D-GISAXS profiles were extracted along the q_y direction for different q_z points (for q_z from 0.69 to 1.52 nm^{-1}), then the 1D-GISAXS profiles were converted to Kratky curves (Iq_y^2 x q_y) in order to model the shapes of agglomerates or crystallites as spheroids with different dimensions [23-25]. Fig. 8 shows the raw data and the Kratky curves fitted according to equation 7 to be presented in the following. They show similar profiles for the samples annealed at 1000°C by RTP and the curve which corresponds to the sample annealed by LASER presents lower intensity. Additionally, this figure also shows that the maximum peak of the Kratky curve is located at lower q_y for the LASER treated films than for the RTP treated films and, according to literature [25,37], the maximum peak at higher $q_y = q_{y,max}$ corresponds to a characteristic wavelength in the plane of the films $d=2\pi/q_{y,max}$, which is at approximately 5.5nm for RTP annealed dielectrics and at approximately 7.2nm for LASER annealed dielectrics. These values are of the same order of size observed by Yang at al. [13] for similar hafnium aluminate films analyzed by electron transmission electron microscopy (TEM).

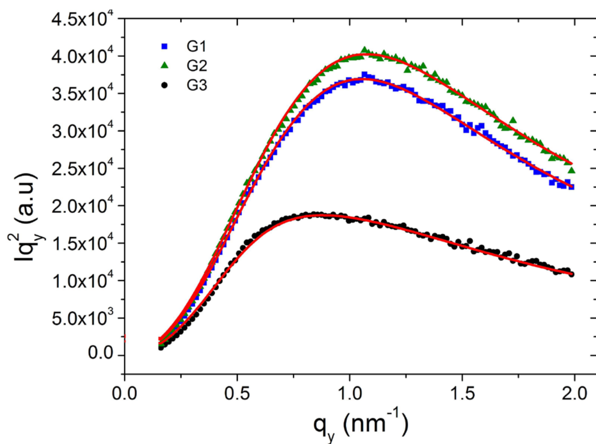

Figure 8. Kratky plot of one-dimensional GISAXS at q_z = 15.82 nm^{-1} of dielectrics annealed by RTP (G1, G2) and annealed by laser (G3). Solid line are the simulated curves using the three particles type.

On the other hand, although the crystallites or agglomerates in the film annealed by LASER are larger, its low scattering intensity indicates that the quantity of them is less than in those annealed by RTP, because the scattering intensity is proportional to the number of centers of scattering [20,36]. The profiles of the Kratky curves point out to the coexistence of different features described by different gyration radius yielding scattering profiles with polydispersive behavior [26,39-41]. In order to investigate the morphological features formed by phase separation into the dielectrics, the Kratky plots were fitted by modeling the hafnium aluminate films with one, two or three types of non-interacting agglomerates. A fitting with an excellent agreement was only possible if three types of agglomerates were included in the model. This model regards that [25]: (a) the total scattering intensity of the system are the total sum of the individual contribution of each type of agglomerates; (b) each type of agglomerates is locally non-interacting, but the total system can interact so that the total scattering intensity behaves as a polydispersive system; (c) the scattering intensity of each type of individual agglomerate obeys to the generalized form of the Ornstein-Zernike (OZ) relation, similar to that employed for Shimizu et al. [24]. The total scattering intensity from the hafnium aluminate layers is the result of the partial contribution of these localized centers of scattering ,weighted by their volumetric fraction (f_k) [25], as describe by equation 7 in which the generalized OZ relationship was included:

$$I(q_y) = \sum_{j=1}^{N=3} f_j I_j = I_0 \sum_{j=1}^{N=3} \frac{f_j}{1+(\xi_j q_y)^{n_j}} \tag{7}$$

where ξ_k is the correlation length and n_k is the fractal dimension of the centers of scattering (n =1, elongated; n =2, flatted or Gaussian chain-like; n =3, sphere-like with fractal surface; n = 4, hard spheres, i.e they can not overlap and have sharp borders) [20,24,25,41]. Although equation 7 was derived regarding non-interacting centers (condition b), it is important to highlight that OZ equation take into account the interaction of the centers, therefore, this equation can adequately describe polydispersive systems [42,43].

The gyration radius, i.e. the root mean square value of the distances of any point in the shape volume of the agglomerates from its center of mass, is obtained from the correlation length as in equation 8:

$$R_{gj} = \xi_j (3)^{1/n_j} \ , j = 1,2,3 \tag{8}$$

The Kratky curves were well fitted with three spheres composed by at least one hard sphere (n_k = 4) and two rougher surface one (3 < n_k < 4) [24,25,40,42] in equation 6, a representative average sphere radius R_k (k = 1,2,3) was computed by equation 9.

$$R_j = \left(\sqrt{\frac{5}{3}}\right)(3)^{1/n_j} R_{gj} \tag{9}$$

The results of the fitting procedure are placed in Table IV and shows that the larger centers of scattering extracted by Kratky maximum peak can be separated in three smaller spheroids with radius varying between 1.14 to 2.67 nm. The exponential parameter n_j of this set of spheroids varies between 3.3 and 4.0, showing that the morphological features in the film have spherical shape with rougher surfaces or even with sharp interfaces. Also, the average radius R_1 R_2 and R_3, extracted from equation 7, indicate a small increase of the average radius for the LASER treatment.

From these results, the morphology of the hafnium aluminate films annealed by RTP (samples G1 and G2) can be modeled as an arrangement of three types of spheroids to represent the morphology of the phase separation after the thermal treatments. It is important to highlight that although the R_j value extracted by fitting the Kratky plot suggests the system to be composed by spheroids with different sizes, they can be understood as localized crystalline agglomerates of

Table V. Parameters extracted fitting the by Kratky plot using the three different spheroidal shapes

Sample	n_1	R_1	f_1	n_2	R_2	f_2	n_3	R_3	f_3
G1	3.9	1.83	0.6	4.0	2.02	0.3	4.0	1.14	0.1
G2	3.5	1.95	0.8	3.1	2.09	0.2	4.0	1.57	0.0
G3	4.0	2.63	0.7	3.9	2.39	0.1	3.25	1.69	0.2

spheroids with different sizes (1.1-2.2 nm) and with different crystalline phases.

As already mentioned before, although the centers of scattering formed in the film annealed by LASER are larger, its low scattering intensity indicates that the quantity of them is less than in those annealed by RTP, because the scattering intensity is proportional to the number of particles [18,19]. In addition, the absence of HfO_2 peaks in the GIXRD spectra of the samples annealed by LASER (sample G3) shows that this compound remains predominantly in amorphous phase with crystalline facets of $Al_{2.4}O_{3.6}$. As a result, considering that GISAXS also points out the existence of centers of scattering, the system can be interpreted as larger (1.7-2.7 nm) spheroids of crystalline $Al_{2.4}O_{3.6}$ embedded in an amorphous matrix.

According to the literature for similar systems [8,13,34], the size of the nanoparticles depends on the Al concentration within the film. Lower concentrations of Al yields bigger nanoparticles, while high concentration of this element leads to the formation small nanoparticles with complex geometry with dimensions within the same order here obtained (≈ 6 nm)[8,34]. On the other side, in addition to the Al concentration dependence of the nanoparticle formation, our results highlight that the phase separation depends on the annealing method as well as of the composition of the annealing atmosphere.

IV. CONCLUSIONS

Hafnium aluminates films with 50 mol% of Hf were deposited onto Si(100) using atomic layer deposition. The films were annealed by RTP at 1000 ºC for 60 s in pure N_2 or N_2+5%O_2 and by LASER at 1200 ºC for 1 ms in pure N_2.

The XRR curves were fitted using the PARRAT32 code [29] that also takes into account the roughness effect upon the reflectivity. The fitting was performed using a four-layer model since the films were non-homogeneous in depth, because a interdiffusion effect was observed during the thermal treatments.

For the films annealed by RTP in N_2, phase separation takes place, promoting the formation of HfO_2 and $Al_{2.4}$ $O_{3.6}$ crystalline phases. In contrast, the films annealed by LASER remain predominantly amorphous with crystalline facets of $Al_{2.4}O_{3.6}$. Also, non-homogeneous distribution of the chemical elements within the dielectrics gave rise to the formation of several regions which can be viewed as sub-layers, each of them with arbitrary electron density and thickness. As a result, Kratky curves pointed out to the coexistence of different features described by different gyration radius yielding GISAXS scattering profiles with polydispersive characteristics.

Finally, the samples annealed by RTP were interpreted as agglomerates of spheroids with different sizes in the range of 1.1 to 2.2 nm and with different crystalline phases whereas the samples annealed by LASER were interpreted as larger spheroids of crystalline $Al_{2.4}O_{3.6}$ (1.7-2.7 nm) embedded in a matrix predominantly amorphous. From CMOS technology point of view, LASER annealing method is more suitable for gate dielectric application because diminish the undesirable phase crystalline separation, even at temperature as great as 1200°C during 1ms.

ACKNOWLEDGEMENTS

The authors would like to acknowledge Brazilian Synchrotron Light Laboratory (LNLS) for the XRR and GISAXS experiments. The authors would also like to thank LAMFI-IFUSP for the RBS measurements. Danilo Roque Huanca was supported by a post doctoral scholarship under the FAPESP process number 2010/09509-5.

REFERENCES

[1] J. Robertson, “High dielectric constant gate oxides for metal oxide Si transistors”, *Reports on Progress in Physics*, vol. 69, no. 2, February G. D. Wilk, R. M. Wallace, and J. M. Anthony, “High-k gate dielectrics: Current status and materials properties considerations”, *Journal of Applied Physics*, vol. 89, no. 10, May, 2010, pages. 5243-5275.

[2] M. Wu, Y. I. Alivov, and H. Morkoç, “High-k dielectrics and advanced channel concepts for Si MOSFET”, *Journal of Materials Science: Materials in electronics*, vol. 19, 2008, pages 915-951.

[3] M. T. Bohr, R. S. Chau, T. Ganhi, and K. Mistry, “The High-k solution”, *Spectrum*, October, 2007, pages 29-35.

[4] M. Houssa, and M. M. Heyns, *High-k Gate Dielectrics, M. Houssa*, Bristol and Philadelphia: 2004, pages 3-13.

[5] R.J. Potter, P. A. Marshall, P. R. Chalker, S. Taylor, A. C. Jones, T. C. Q. Noakes, and P. Bailey, “Characterization of hafnium aluminate gate dielectrics deposited by liquid injection metalorganic chemical vapor deposition”, *Applied Physics Letters*, vol. 84, no. 20, May, 2004, pages. 4119-4121.

[6] D. M. Hausmann, E. Kim, J. Becker, and R. G. Gordon, “Atomic layer deposition of hafnium and zirconium oxides using metal amide precursor”, *Chemistry of Materials*, vol. 14, no. 10, September, 2002, pages 4350-4358.

[7] M.-Y. Ho, H. Gong, G. D. Wilk, B. W. Busch, M. L Green, P. M. Voyles, D. A. Muller, M. Bude, W. H. Lin, A. See, M. E. Loomans, S. K. Lahiri, P. I. Räisänen, “Morphology and crystallization kinetics in HfO_2 thin films grown by atomic layer deposition”, *Journal of Applied Physics*, vol. 93, no. 3, February, 2003, pages 1477-1481.

[8] E. P. Gusev, C. Cabral Jr, M. Copel, C. D’Emic, M. Gribelyuk, “Ultrathin HfO_2 films grown on silicon by atomic layer deposition for advanced gate dielectrics application”, *Microelectronic Engineering*, vol. 6, no. 2-4, September, 2003, pages 145-151.

[9] T. Nishimura, T. Okazawa, Y. Hoshino, Y. Kido, K. Iwamoto, K. Torminaga, T. Nabatame, and A Toriumi, “Atomic scale characterization of HfO_2/Al_2O_3 thin films grown on nitride and oxidized Si substrate”, *Journal of Applied Physics*, vol. 96, no. 11, December, 2004, pages 6113-6119.

[10] N. Mommer, T. Lee, and J. A. Gardner, “Stability of monoclinic and tetragonal zirconia at low oxygen partial pressure”, *Journal of Materials Research*, vol. 15,no. 2, January, 2000, pages 377-381.

[11] X. Zhao, and D. Vanderbilt, “First-principles study of structural, vibrational, and lattice dielectric properties of hafnium oxide”, *Physical review* , vol. 65, no. 23, June, 2002, 085107.

[12] S. Stemmer, Y. Li, B. Foran, P. S. Lysaght, S. K. Streiffer, P. Fuoss, and S. Seifert, “Grazing-incidence small angle x-ray scattering studies of phase separation in hafnium silicate films”, *Applied Physics Letters*, vol. 83, no. 15, October, 2003, pages 3141-3143.

[13] Y. Yang, W. Zhu, T. P. Ma, and S. Stemmer, “High-temperature phases stability of hafnium aluminate films for alternative gate dielectrics”, *Journal of Applied Physics*, vol. 95, no. 7, April, 2004, pages 3772-3777.

[14] T. Wang, and J. G. Ekerdt, “Structure versus thermal stability: the periodic structure of atomic layer deposition-grown Al-incorporated HfO_2 films and its effects in amorphous stabilization”, *Chemistry of Materials*, vol. 23, no. 7, April, 2011, pages 1679-1685.

[15] P. F. Lee, J. Y. Dai, K. H. Wong, H. L. W. Chan, and C. L. Choy, “Study of interfacial reaction and its impact on electric properties of Hf-Al-O high-k gate dielectric thin films grown on Si”, *Applied Physics Letters*, vol. 82, no. 15, April, 2003, pages 2419-2421

[16] A. G. Cullis, “Transient annealing of semiconductors by laser, electron beam and radiant heating techniques”, *Reports on Progress in Physics*, vol. 48, no. 8, August, 185, pages 1155-1233.

[17] U. M.Bhatta, J. Ghatak, M. Mukhopadhyay, R. Conley, C. Liu, P. V. Satyam, “Structural analysis of DC magnetron sputtered and spin coated thin films using RBS, TEM, and X-ray reflectivity methods”, *Nuclear Instruments and Methods in Physics Research SectionB: Beam Interactions with Materials and Atoms*, vol. 266, no. 8, April, 2008, pages 1548-1552.

[18] C. Wyon, J. P. Gonchond, D. Delille, A. Michallet, J. C. Royer, L. Kwakman, and S. Marthon, “X-ray metrology for advanced silicon process”, *Applied Surface Science*, vol. 253, no. 1, October, 2006, pages 21-27.

[19] R. Lazzari, *X-ray and Neutron Reflectivity: Grazing Incidence Small-Angle X-ray Scattering from Nanostructures*, Editors J. Daillant, and A. Gibaud, Springer, Berlin: 2009, pages 283-342.

[20] P. Müller-Buschbaum, *A Basic Introduction to Grazing Incidence Small-Angle, in Applications of Synchrotron Light to scattering and Difraction in Materials and Life Science*, Editors M. Gomez, A. Nogales, M. C. Garcia-Gutierrez,and T. A. Ezquerra, Springer, Berlin Heidelberg: 2009, pages 61-89

[21] S. Terada, H. Mrakami, K. Nishihagi, and H. Osaka, “Thickness and density measurement for new materials with combined X-ray technique”, in *Proceedings of the Advanced Semiconductor Manufacturing Conference*, 2001 IEEE/SEMI, pages 125-130.

[22] M. Meuris et al., in IEEE International Semiconductor Manufacturing Conference Proceedings/1999, p. 157, IEEE, Piscataway, NJ (1999).

[23] T. Salditt, D. Lott, T. H. Metzger, J. Peisl, G. Vignaud, P. Ho/go/j, O. Schärpf, P. Hinze, and R. Lauer, “Interfacial roughness and related growth mechanisms in sputtered W/Si multilayers”, *Physical Review B*, vol. 54, no. 8, June, 1996, pages 5860-5872.

[24] W. Shimizu, J. Hokka, T. Sato, H. Usami, and Y. Murakami, “Microstructure investigation on micropore formation in microporous silica materials prepared via catalytic sol-gel process by small angle X-ray scattering”, *The Journal of Physical Chemistry B*, vol. 115, no. 30, June, 2011, pages 9369-9378.

[25] D. I Svergun, and M. H. J. Koch, “Small-angle scattering studies of biological macromolecules in solution”, *Reports on Progress in Physics*, vol. 66, no. 10, October, 2003, pages 1735-1782.

[26] G. Glatter, and O. Kratky, *Small Angle X-ray Scattering*, Academic Press, New York (1982).

[27] M. Mayer, “SIMNRA, a simulation program for the analysis of NRA, RBS and ERDA”, in *AIP Conference Proceeding*, vol. 475, 1999, pages 541-544.

[28] U. Pietsch, V. Holy, and T. Baumbach, *High-Resolution X-ray Scattering: From thin Films to Lateral Nanostructures*, Springer-Verlag, New York: 2004, pages 143-178.

[29] A. Gibaud, and G.Vignaud, *X-ray and Neutron Reflectivity: Specular Reflectivity from Smooth and Rough Surfaces*, editor J. Daillant, A. Gibaud, Springer, Berlin Heidelberg: 2009.

[30] C. Braun, Parrat32, version 1.6, HMI Berlin, Berlin: 2002. http://www.hmi.de/bensc/instrumentation/instrumente/v6/refl/parratt_en.htm.

[31] L. G. Parratt, “Surface studies of solids by total reflection of X-rays”, *Physical Review*, vol. 95, no. 2, July, 1954, pages 359-369.

[32] L. Névot , and P. Croce, “Caractérisation des surfaces par réflexion rasante de rayons X. Application à l’étude du polissage de quelques verres silicates”, *Revue de Physique Appliquée*, vol. 15, no. 3, march, 1980, pages 761-779.

[33] S. M. George, “Atomic layer deposition: An overview”, *Chemical Review*, vol. 110, no.1, November, 2010, pages 111-131.

[34] J. Y. Dai, K. Li, P. F. Lee, X. Zhao, and S. Redkar, “STEM study of interfacial reaction at $Hf_xAl_{1-x}O_y$/Si interfaces”, *Thin Solid Films*, Vol. 462-463, September, 2004, pages 114-117.

[35] R. Schmid, W. Hosler, and R. Tilgner, “RBS measurement of the thickness od nanometer oxide layers: adhesion strength between copper leadframe and molding compound correlated with the oxide layer thickness”, in *Proceeding of Electronic Packing Technology Conference*, 1997, pages 188-193.

[36] P. J. Morh, and B. N Taylor, *Fundamental Physical Constants*, in *CRC Handbook of Chemistry and Physics 87th*, D. R. Lide editor, California, U. S. A , 2006

[37] G. Renaud, R. Lazzari, and F. Leroy, “Probing surface and interface morphology with gazing incidence small angle X-ray scattering”, *Surface Science Reports*, vol. 64, no. 8, August, 2009, pages 255-380.

[38] Y. Yoneda, “Anomalous surface reflection of X-rays”, *Physical Review*, vol. 131, no. 5, September, 1963, pages 2010-2013.

[39] A. Guinier, *X-ray Diffraction in crystals imperfect crystals, and amorphous bodies*, W. H. Freeman and Company, U. S. A (1963)

[40] R. P. Rambo, and J. A. Tainer, “Improving small angle X-ray scattering data for structural analyses of the RNA world”, *RNA*, vol. 16, no. 3, March, 2010, pages 638-646.

[41] C. D. Putman, M. Hammel, G. L. Hura, and J. A. Tainer, “X-ray solution scattering (SAXS) combined with crystallography and computation: defining accurate macromolecular structures, conformations and assemblies in solution”, *Quarterly Reviews of Biophysics*, vol. 40, no 3, 2007, pages 191-285.

[42] D. Case, F. R. Manby, “The Ornstein-Zernike equation in molecular electronic structure theory” Molecular Physics, vol. 108, no. 3-4, February, 2010, pages 307-314.

[43] M.-L. Che, S. Chuang, J. Leu, “The mechanical property, microstructure, and pore geometry of a methyltrimethoxysilanemodified silica zeolite (MSZ) film”, *Journal of the Electrochemical Society*, vol. 159, no. 3, mm,2012, pages G23-G28.